Out-of-Plane Compression Behaviour of Honeycomb Structures with Mass Gradient Produced by Additive Manufacturing Technologies

Tiago Rua

tiagovrua@tecnico.ulisboa.pt

Instituto Superior Técnico – University of Lisbon, Portugal

September 2021

Abstract: The present work has as its main objective to evaluate the out-of-plane behaviour on functionally graded cellular materials – namely honeycomb structures – under compressive conditions. The study is conducted both experimentally and numerically, using the software ABAQUS 2017. The experimental specimens were produced out of PLA and aluminium using Additive Manufacturing techniques – Fused Filament Fabrication (FFF) and Selective Laser Melting (SLM), respectively. The studied geometries were modelled with uniform wall thickness (regular structures) and with varying wall thickness and cell length size through different geometrical variations (graded structures). The study showed verified that in-plane geometrical parameters influence how the structure (whether regular or graded) handled with out-of-plane loadings: larger structure's overall size and larger thickness-to-length ratio enhance the energy absorbed and the stiffness in an out-of-plane loading. The strength of the structure is increased by the enhancement of the relative density (related to the thickness-to-length ratio). The introduction of in-plane geometrical gradients promotes the improvement of energy absorption and stiffness: higher mass concentrations near the structure's centre tend to perform better in comparison to non-graded structures. Regarding PLA models, there was a good agreement between experimental and numerical values, which not only indicates that the production of PLA cellular materials through FFF is a good option, but also validates the Finite Element Method as an alternative to experimental testing when it comes to evaluate new designs. Relatively to the aluminium samples, it was not possible to make any affirmations regarding the potential of SLM or validate the numerical analysis due to incongruences detected in the experimental values.

Keywords: Functionally Graded Materials, Honeycomb Structures, Additive Manufacturing, Finite Element Analysis, Out-of-plane loading, Energy Absorption.

1. Introduction

Composite materials are defined as a mixture of two (or more) different types of materials, combined into one. The principal benefit from this combination is the achievement of better mechanical properties, providing new materials with high strength-to-weight ratio. These materials are constituted by a matrix, which is the main material, and a reinforcement phase in forms of particles, fibres or sheets [1]. A very well-known composite structure is the sandwich panel, which is composed by a core embedded between two exterior sheets. The core can have several designs, such as foam, honeycomb, tetrahedral truss or lattice structures, among others [2-6]. Many core structures are also inspired in biological geometries [2]. The focus of the study will be on honeycomb hexagonal structures.

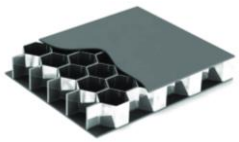

Figure 1 - Sandwich structure with honeycomb core [7].

Honeycomb structures are well known for their capability to absorb high quantities of energy and their high strength-to-weight ratio [8, 9]. This type of structures has also good properties when it comes to thermal and acoustic isolation, and radio frequency shielding [10]. All these properties enable them to be applied in industries such as aerospace, transportation sector [10], civil construction and marine [2]. In the later years, honeycomb structures have become a solution for tissue engineering and regenerative medicine, in particular for designing scaffolds, making possible tissue regeneration [11]. The biocompatibility, biodegradability and processability of cyto-compatible hydrogels capable of 3D cell encapsulation are attractive characteristics for tissue regeneration purposes [11].

Additive manufacturing (AM) plays an important role on cellular materials production. The advances on AM techniques have made more feasible the production of geometries that make use of cellular materials [3-6, 12]. The possibility to make complex geometries and rapid prototyping, allied to a constant decrease in 3D printing

costs [13, 14] have made AM very attractive to produce cellular materials, especially on aerospace and medical areas [13-15]. For this work, Fused Filament Fabrication (FFF) and Selective Laser Melting (SLM) were used to produce the PLA and the aluminium specimens, respectively.

SLM is a powder-bed fusion process, where metallic particles in a powder-bed are melted using a high intensity laser beam, welding these particles to form a specimen with a defined geometry. Only metallic materials can be applied to SLM processing. As the material is powdered, it is possible to mix different metallic materials, resulting in final materials with better mechanical properties.

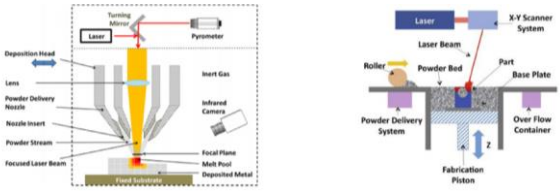

Figure 2 - Schematics of the powder-bed fusion process [15].

Fused Filament Fabrication (FFF), adapted from a patented technology called Fused Deposition Modeling (FDM), is a process where the material is pre-heated to its melting temperature, leaving the extruder nozzle, which has a free 2D movement to draw the geometry layer by layer into a heated build plate. As a layer is being cooled to the material's solidification point, a new one is being constructed on top of that.

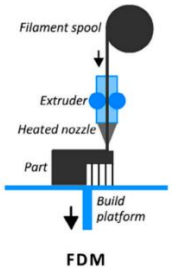

Figure 3 - Schematics of FFF process [16].

At this work, several regular and graded structures were designed. One of the main design parameters was the thickness-to-length ratio, which is directly linked to the relative density ($\bar{\rho}$). This is one of the key properties to distinguish different cellular materials. It can be defined by a fraction between the volume of solid material (V_s) contained on a reference volume (V_{ref}) and the reference volume [9]. This reference volume may be set around a vertex common to various unit cells (figure 4). Given the core structure is a two-dimensional entity, this fraction may even be simplified to the area of solid material (A_s) over the reference area (A_{ref}). This deduction is detailed on equation 1, where m_s stands for the mass of solid [9]:

$$\bar{\rho} = \frac{\rho^*}{\rho_s} = \frac{m_s}{V_{ref}} * \frac{V_s}{m_s} = \frac{V_s}{V_{ref}} \Leftrightarrow \bar{\rho} = \frac{A_s}{A_{ref}} \quad (1)$$

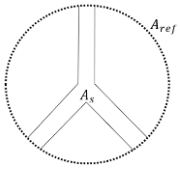

Figure 4 - Reference area on a unit cell.

2. Materials and Methodology

2.1 Materials

The test specimens were produced using PLA (through FFF) and aluminium alloy AlSi7Mg0,6 (through SLM). The considered properties for both materials are displayed on tables 1 and 2.

Table 1 - Considered PLA properties for the study.

Density [g/cm^3]	Young's Modulus [MPa]	Poisson Ratio	Yield Strength [MPa]	Tensile Strength [MPa]
1.252	1500	0.36	25	51

Table 2 - Considered aluminium properties for the study.

Density [g/cm^3]	Young's Modulus [MPa]	Poisson Ratio	Yield Strength [MPa]	Tensile Strength [MPa]
2.680	59000	0.33	211	375

2.2 Structures design

Figure 5 illustrates the two design geometrical parameters: cell length (l) and wall thickness (t).

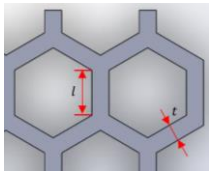

Figure 5 - Schematics of the unit cell and geometric variables.

Regular Structures

Regular structures have their wall thickness uniform throughout the entire structure. The thickness was kept at 2,31 mm, with the core height (h) varied between 6 mm, 10 mm and 12 mm and with two different overall specimen sizes (the projected area). Table 3 details the characteristics of the designed regular structures.

Table 3 - Characteristics of the hexagonal regular structures.

l [mm]	h [mm]	Specimen size [mm^2]	$\bar{\rho}$
4 ("L4")	6	48.51 x 48	0.439
	10		
	12		
	6	66.99 x 64	0.438
	10		
	12		
6 ("L6")	6	48.51 x 48	0.338
	10		
	12		
	6	66.99 x 64	0.331
	10		
	12		
8 ("L8")	6	50.82 x 56	0.273
	10		
	12		
	6	83.15 x 84	0.269
	10		
	12		
10 ("L10")	6	61.20 x 68	0.228
	10		
	12		
	6	100.46 x 102	0.225
	10		
	12		

Figures 6 and 7 show the larger PLA and aluminium specimens of for each cell length geometries.

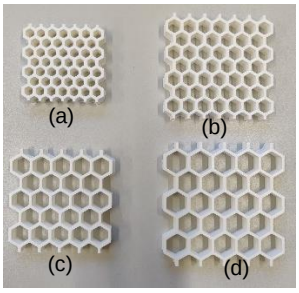

Figure 6 - PLA Specimens of geometries (a) L4, (b) L6 (c) L8, (d) L10.

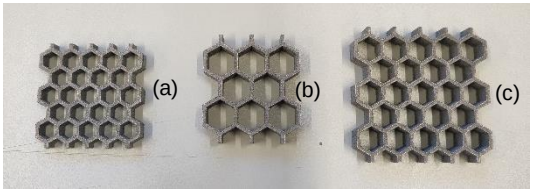

Figure 7 - Aluminium Specimens of geometries (a) L6, (b) L8, (c) L10.

Graded Structures

Several geometries were made as a result of three different design methods. The structures are divided in groups according to their design methods. The gradient was introduced with changes in the wall thickness and cell length.

In the first design method, the cell length was imposed, varying between 6, 8 and 10 mm in two ways: increasing (6-8-10) and decreasing (10-8-6) from the centre to the borders. The core height was kept constant. Table 4 shows the graded structures of the first design method.

Table 4 - Characteristics of the graded structures (1st design method).

Configuration	h [mm]	Specimen size [mm^2]	$\bar{\rho}$
6 – 8 – 10 ("T6-8-10")	12	91.59 x 91.35	0.322
10 – 8 – 6 ("T10-8-6")	12	91.57 x 91.14	0.421

In the second design method, a constant variation of the cell length (± 0.5 mm) was imposed, maintaining the core height. Two options for the increment and another two for the decrement of the cell length were designed. Table 5 shows the graded structures of the second design method.

Table 5 - Characteristics of the graded structures (2nd design method).

Configuration	h [mm]	Specimen size [mm^2]	$\bar{\rho}$
Decreasing density (1) ("S0.5+_1O")	12	100.46 x 102	0.443
Decreasing density (2) ("S0.5+_2O")	12	100.46 x 102	0.466
Increasing density (1) ("S0.5+_1O")	12	100.46 x 102	0.426
Increasing density (2) ("S0.5+_2O")	12	100.46 x 102	0.410

In the third design method, the cell length and the wall thickness were both dependent on the gradient parameter, R_1. The R_1 parameter defines the cell length increment along the main symmetry lines, as a result of the first increment – from the centre cell to the immediately next ones. The parameter is the slope of a linear function of two fractions: $\frac{x_i}{L^*}$ versus $\frac{d_i}{l}$, where L^* represents the distance from the more distant wall of the centre cell to the side end of the core, x_i represents the distance from the origin of the length L^* to the end of the i cell (along a main symmetry line of the structure), and d_i represents the in-plane thickness of the i cell, l represents half of the base cell length. Figure 8 shows the geometric parameters mentioned above.

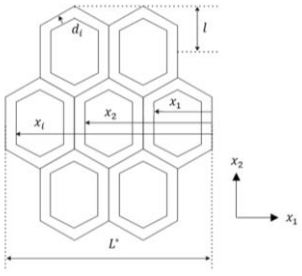

Figure 8 - Considered measure variables for R1 calculation.

Table 6 details the designed geometries for the third design method. The core height was kept constant.

Table 6 - Characteristics of the graded structures (3rd design method).

R_1	h [mm]	Specimen size [mm²]	$\bar{\rho}$
+0.22	12	88.51 x 90	0.323
+0.31	12	88.51 x 90	0.265
+0.37	12	88.51 x 90	0.199
-0.22	12	88.51 x 90	0.240
-0.31	12	88.51 x 90	0.298
-0.37	12	88.51 x 90	0.199

Figures 9 shows the larger specimens of PLA and aluminium for each cell length geometries.

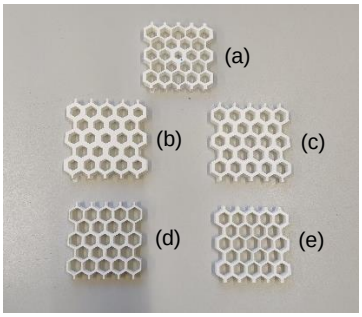

Figure 9 - PLA specimens of graded structures: (a) "T6-8-10"; (b) "S0.5+_2O"; (c) "S0.5-_2O"; (d) "R_1 = +0.31"; (e) "R_1 = -0.31".

2.3 Numerical model

The numerical analysis was done following the Finite Element Method on software *ABAQUS 2017*. The model replicates the uniaxial compression test. For that, three instances were created on the model: the two compression plates of the test setup and the honeycomb structure. A mesh convergence analysis was done prior to the simulations in order to refine the mesh for better results. The boundary conditions were set as follows: the lower plate is totally fixed, while the upper plate moves to an imposed displacement of 0.5 mm. The plates have their material defined with the Young's Modulus infinitely higher than the structure's one, inducing all deformation over the structure. Regarding the mechanical regime of the simulations, the following was set up: for the PLA regular models, only-elastic and elasto-plastic simulations were done; for the PLA graded structures and aluminium regular structures, an only-elastic simulation was done.

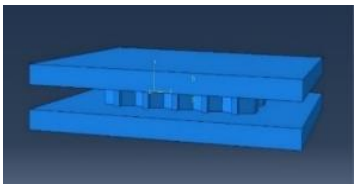

Figure 10 - Numerical model assembly for all honeycomb structures.

2.4 Experimental testing

The experimental tests were carried at Laboratório de Mecânica Experimental – Departamento de Engenharia Mecânica, Instituto Superior Técnico. The PLA and aluminium specimens were submitted to a uni-axial compression test, according to the ASTM C365-94 [17] standard. and the equipment used at the was an Instron 3369, with a load cell of 50 kN (visible on figure 11).

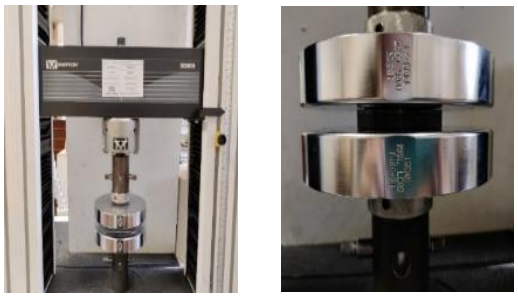

(a) (b)

Figure 11 - (a) Instron 3369; (b) load cell of 50 kN.

Different tests were performed regarding the material's mechanical regime. For PLA samples, the tests were performed under elasto-plastic regime until failure. For the aluminium samples, the test was performed with an imposed displacement of 0.5 mm. All the tests were performed at a constant speed of 0.5 mm/min. It is important to clarify that not all 3D modelled geometries were submitted to test.

3. Results and Discussion

3.1 Preliminary Notes

It is important to refer some aspects regarding the methodology and the physical aspects of the specimens produced for this work. Regarding the specimens production, it shall be noted that:

- On aluminium specimens, a large porosity was noted inside the cell walls, which could eventually lead to structures with different densities rather than the expected. This may lead to non-relatable experimental values on the studied variables in comparison to the numerical values. In addition to this, some imperfections at the ends of the structures were also noted;
- The filament roll was changed in between the production of the PLA structures. Although the used material has no difference between rolls, this may result in values discrepancies over the studied variables;

- Yet in some PLA specimens, there were noticed some infill gaps. This happens due to the lack of concordance between the printing raster and the wall thickness. Hence, it may induce some less conservative results when evaluating the performance of the 3D-printed structures.

Finally, in what concerns to the mechanical properties of PLA, the considered Young's Modulus for the numerical analysis was an average between the considered values from two previous works [4, 18] with their PLA material purchased to the same supplier. Therefore – plus the fact that there is no technical data sheet from this material's manufacturer – it is not guaranteed that the Young's Modulus implicit on both numerical and experimental data are the same.

3.2 Force vs. Displacement curves

In this section, the force vs. displacement curve of each case is presented. From these, the values of specific stiffness[1], specific energy absorbed[2] and specific stress[3] (through the calculation of the force at $\Delta = 0.1$ mm over the solid area of the structure, at a fixed displacement of 0.1 mm for every structure) are taken as study variables. "NUM_OE" refers to only-elastic mechanical regime simulation, "NUM_EP" refers to elasto-plastic mechanical regime simulation and "EXP" refers to experimental result.

PLA Regular Structures

Figures 12 and 13 show the force vs. displacement curves of the "L4 – 48.51 x 48" at core heights 6, 10 and 12 mm and the "L4 – 66.99 x 64" structures at core height 12 mm. Figure 14 and 15 show the force vs. displacement curves of the "L10 – 61.20 x 68" at core heights 6,10 and 12 mm and the "L10 – 100.46 x 102" at core height 12 mm.

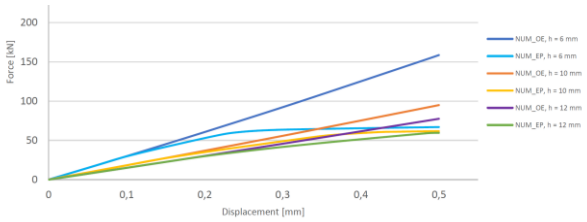

Figure 12 - Force vs. Displacement curve for "L4 - 48.51 x 48" at different core heights - PLA regular structure.

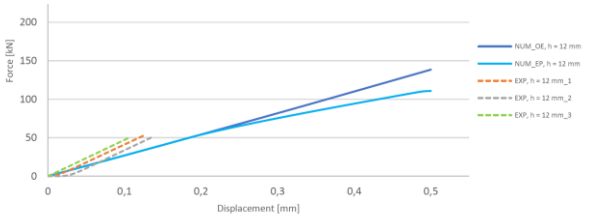

Figure 13 - Force vs. Displacement curve for "L4 - 66.99 x 64" at core height 12 mm - PLA regular structure.

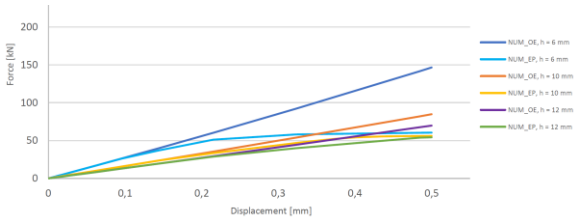

Figure 14 – Force vs. Displacement curve for "L10 – 61.20 x 68" at different core heights – PLA regular structure.

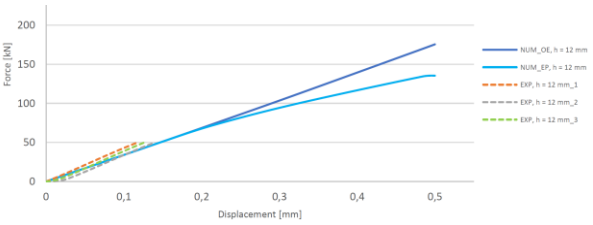

Figure 15 – Force vs. Displacement curve for "L10 – 100.46 x 102" at core height 12 mm – PLA regular structure.

It is possible to verify that, for the L4 model with specimen size 66.99 x 64 mm^2, the maximum force value is higher than the one on the "L4 – 48.51 x 48" structure for the same core height (12 mm). However, the "L10 – 100.46 x 102" structure has higher force values than the "L4 – 66.99 x 64" structure, keeping the same core height (12 mm). Regarding the experimental values on figure 13 and figure 15, it is possible to verify that the slopes of force vs. displacement curves are slightly higher than the numerical ones. Taking into account the core height variation in the L4 and L10 models (figures 12 and 14), it is possible to see that the force decreases with the increment of the height.

PLA Graded Structures

Figures 16 and 17 show the force vs. displacement curves for the "R_1 = +0.31" and "R_1 = -0.31" structures, both with specimen size 88.51 x 90 mm^2, and at core height 12 mm.

[1,2,3] The specific values of these variables mean their normalized value by dividing the relative density of each structure.

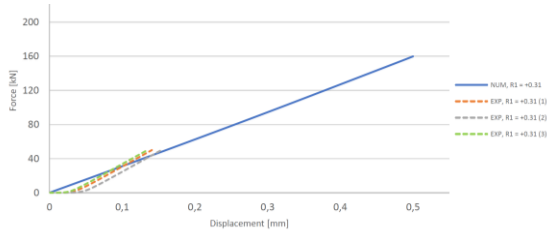

Figure 16 - Force vs. Displacement curve for "R_1 = +0.31" at core height 12 mm – PLA graded structure.

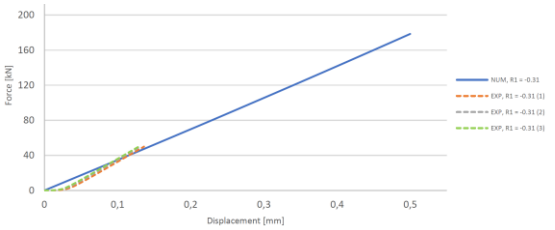

Figure 17 - Force vs. Displacement curve for "R_1 = -0.31" at core height 12 mm – PLA graded structure.

Analysing figures 12 to 17, it is visible that the graded structures are the ones with highest maximum force values. Also, looking at the experimental results, the graded structures show larger displacement for the same force values.

Aluminium Regular Structures

Figures 18 and 19 show the force vs. displacement curves of the "L6 – 65.81 x 66" and the "L8 – 83.15 x 84" structures at core heights 6 and 12 mm. The figures show both numerical and experimental results.

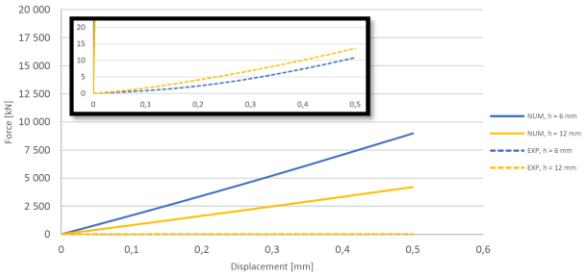

Figure 18 - Force vs. Displacement curve for "L6 – 65.81 x 66" at core heights 6 and 12 mm – Aluminium regular structure.

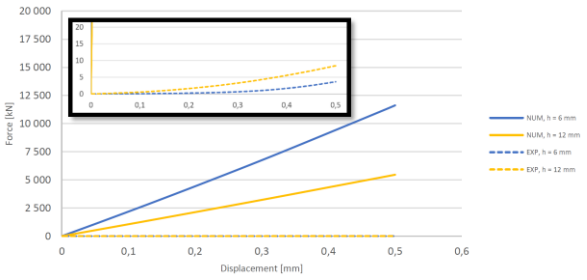

Figure 19 - Force vs. Displacement curve for "L8 – 83.15 x 84" at core heights 6 and 12 mm – Aluminium regular structure.

Looking at the figures above, a large difference in the force values between the numerical and the experimental values is noted. Nevertheless, it is possible to see that the force values on the "L8 – 83.15 x 84" structure are higher than the ones on "L6 – 65.81 x 66". Also, like in PLA regular structures, the difference of force values is noted between different core heights.

3.3 Discussion of the results

Table 7 shows the numerical values of the referred study variables for the PLA structures.

Table 7 - Specific energy absorbed, specific stiffness and specific stress for PLA – numerical analysis.

Model	h [mm]	$\frac{E_a}{\bar{\rho}}$ [kN.mm]	$\frac{K}{\bar{\rho}}$ [kN/mm]	$\frac{\sigma}{\bar{\rho}}$ [MPa]
"L4 – 48.51 x 48"	6	3.11	776	60
	10	1.90	454	39
	12	1.56	368	32
"L4 – 66.99 x 64"	6	5.60	1385	62
	10	3.37	798	38
	12	2.80	656	31
"R_1 = +0.31"	12	4.17	1252	53
"R_1 = -0.31"	12	3.95	1242	50

Table 8 shows the experimental values of the referred study variables for the PLA structures.

Table 8 - Specific energy absorbed, specific stiffness and specific stress for PLA – experimental test.

Model	h [mm]	$\frac{E_a}{\bar{\rho}}$ [kN.mm]	$\frac{K}{\bar{\rho}}$ [kN/mm]	$\frac{\sigma}{\bar{\rho}}$ [MPa]
"L4 – 65.81 x 66"	12	4.64 ± 0.76	1005 ± 92	49 ± 8
"R_1 = +0.31"	12	5.97 ± 0.88	1714 ± 412	53 ± 8
"R_1 = -0.31"	12	5.81 ± 0.29	1630 ± 192	49 ± 2

Reviewing the numerical values for the study variables of PLA regular structures, it is possible to verify that the specimen size has the greatest influence in energy absorption and structure's stiffness: the larger the structure is, the higher the energy absorbed and stiffness are. Although not all the collected data is presented here, further inspection allowed to state the influence of the relative density, but this one with a smaller contribution than the specimen size: structures with higher relative density have enhancement of the energy absorbed and higher stiffness. It is then possible to establish a hierarchy of the geometrical parameters' influence over the structures: in first place, the specimen size, and in second place, the thickness-to-length ratio. Regarding the specific stress, it is only dependent on the relative density of the structures; i.e., the higher the relative density is, the lower the stress felt by the structures are.

The figures 20, 21 and 22 show the identified patterns on all numerically studied PLA regular structures as described above.

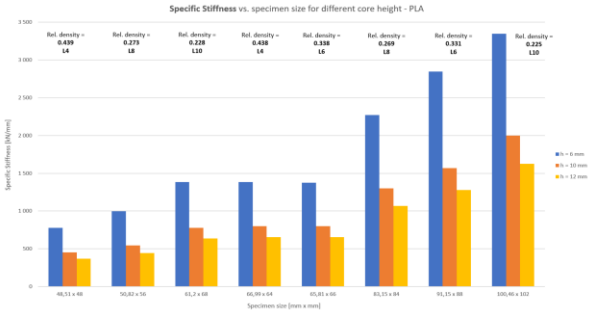

Figure 20 - Specific stiffness vs. specimen size for PLA regular structures – Numerical analysis.

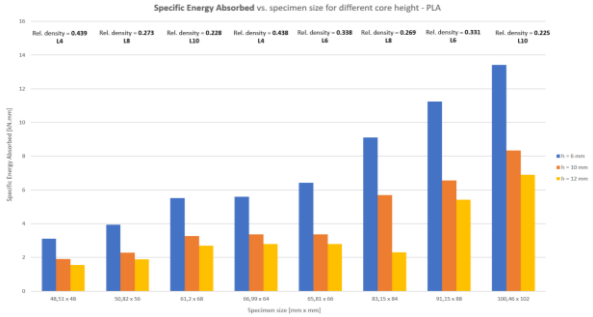

Figure 21 – Specific energy absorbed vs. specimen size for PLA regular structures – Numerical analysis.

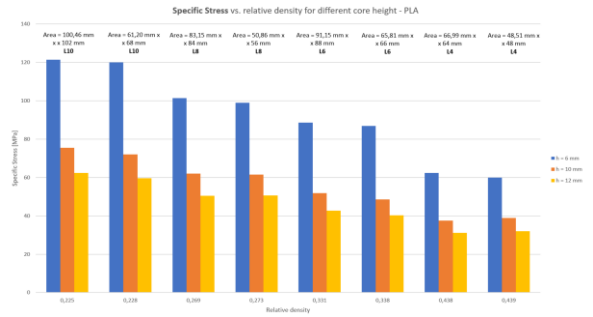

Figure 22 - Specific stress vs. relative density for PLA regular structures - Numerical analysis.

In what concerns to the experimental values for the study variables of PLA regular structures, the relative density influence on energy absorption, stiffness and stress was detected; however, a different pattern for the specific energy absorbed and specific stiffness was identified: these values decrease with the increment of the relative density. Figures 23, 24 and 25 show the described patterns above for all experimentally studied PLA regular structures.

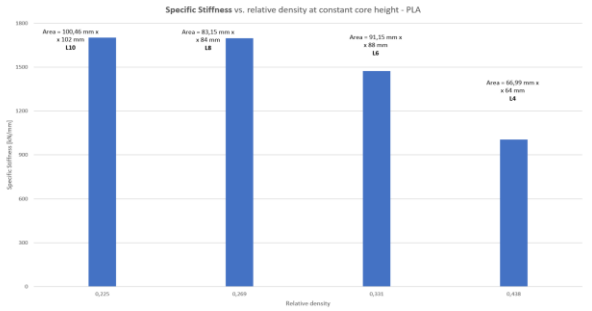

Figure 23 - Specific stiffness vs. relative density for PLA regular structures – Experimental test.

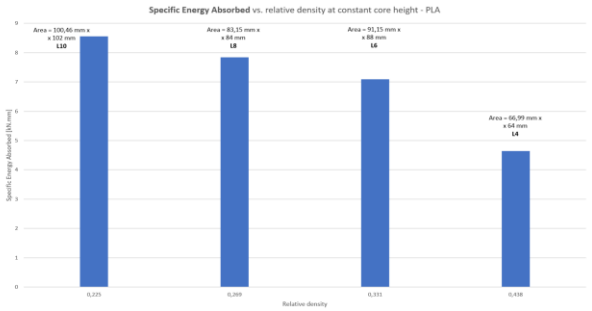

Figure 24 - Specific energy absorbed vs. relative density for PLA regular structures – Experimental test.

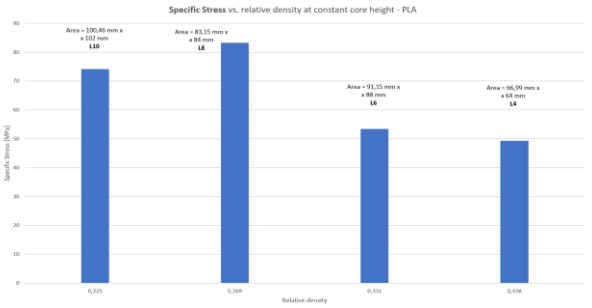

Figure 25 - Specific stress vs. specimen size for PLA regular structures – Experimental test.

Regarding the numerical results for PLA graded structures, the following was observed: the influence of specimen size and relative density over the specific energy absorbed and specific stiffness: these values increase with the specimen size and the thickness-to-length ratio. Once again, the specific stress is only dependent on the relative density: higher relative densities imply lower stresses.

Further inspection into the results of the third design method for graded structures suggest the appearance of another factor to influence the structures performance. Structures with positive gradient and smaller magnitude tend to perform better; i.e., structures with more mass concentration near the centre show improvements in stiffness and energy absorption capacity. Furthermore,

looking at the "R_1 = +0,31" and "R_1 = +0,31", the effect of the magnitude and signal of the gradient is even more visible: even though the "R_1 = -0,31" structure has higher relative density (0.298 against 0.265), both numerical and experimental results point to better performance in energy absorption and improved stiffness for the "R_1 = +0,31". Nevertheless, the specimen size and relative density continue to have greater impact than the mass distribution, overall.

Figure 26, 27 and 28 emphasise the numerical patterns above referred.

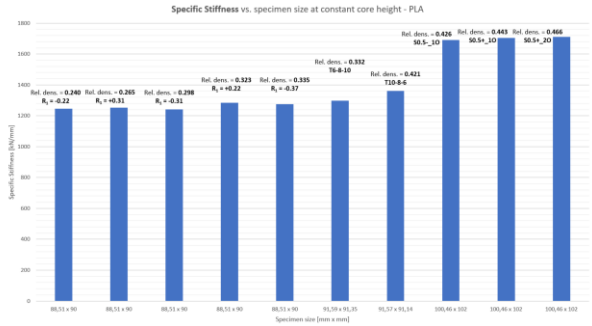

Figure 26 - Specific stiffness vs. specimen size for PLA graded structures – Numerical analysis.

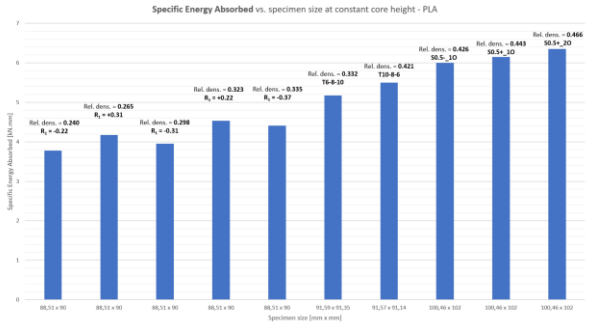

Figure 27 - Specific energy absorbed vs. specimen size for PLA graded structures – Numerical analysis.

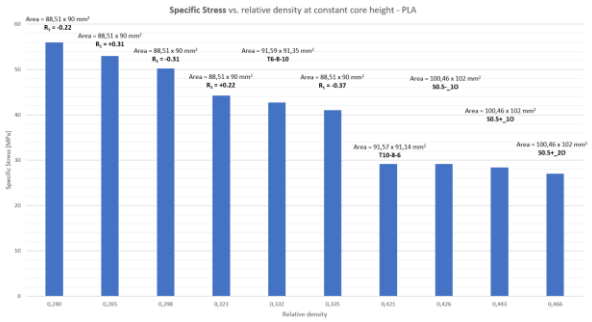

Figure 28 - Specific stress vs. relative density for PLA graded structures – Numerical analysis.

Table 9 shows the numerical values of the referred study variables for the aluminium structures.

Table 9 - Specific energy absorbed, specific stiffness and specific stress for Aluminium– numerical analysis.

Model	h [mm]	$\frac{E_a}{\bar{\rho}}$ [kN.mm]	$\frac{K}{\bar{\rho}}$ [kN/mm]	$\frac{\sigma}{\bar{\rho}}$ [MPa]
"L6 – 65.81 x 66"	6	228	57277	3286
	12	110	26834	1589
"L8 – 83.15 x 64"	6	370	93239	4117
	12	180	42161	1998

Table 10 shows the experimental values of the referred study variables for the aluminium structures.

Table 10 - Specific energy absorbed, specific stiffness and specific stress for Aluminium– experimental analysis.

Model	h [mm]	$\frac{E_a}{\bar{\rho}}$ [kN.mm]	$\frac{K}{\bar{\rho}}$ [kN/mm]	$\frac{\sigma}{\bar{\rho}}$ [MPa]
"L6 – 65.81 x 66"	6	41	74478	1752
	12	95	81026	3391
"L8 – 83.15 x 64"	6	4	74188	150
	12	49	91353	1160

In what concerns to the aluminium results, it is possible to see same pattern as in the PLA regular structures, regarding the specific energy absorbed and the specific stiffness: the specimen size and the relative density are the main factors to influence the stiffness and the energy capacity of the structures. Regarding the specific stress, the previous identified pattern of the relative density is also identified: the higher the relative density is, the lower the stress is. Relatively to the experimental results on aluminium specimens, it isn't possible to make a definite statement about the obtained results due to incongruences not only in the force vs. displacement curves (very low values of force compared to the numerical ones), but also in the study variables values. A large error is noted based on the fraction between the mean value and the highest deviation for the three study variables.

Figure 29, 30 and 31 show the numerical values of specific stiffness, specific energy absorbed and specific stress for the aluminium regular structures.

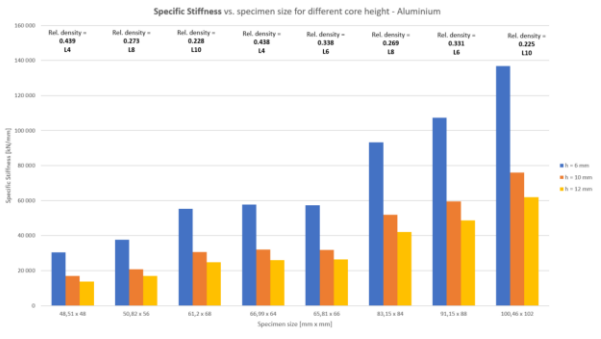

Figure 29 - Specific stiffness vs. specimen size for aluminium regular structures – Numerical analysis.

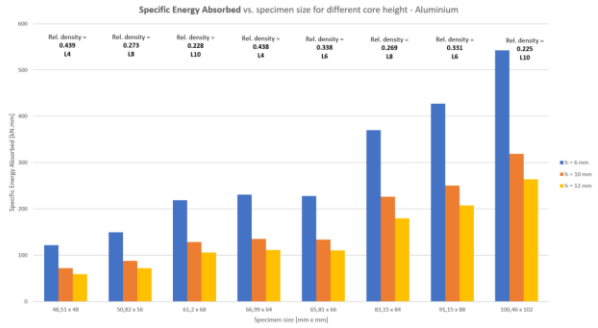

Figure 30 - Specific energy absorbed vs. specimen size for aluminium regular structures – Numerical analysis.

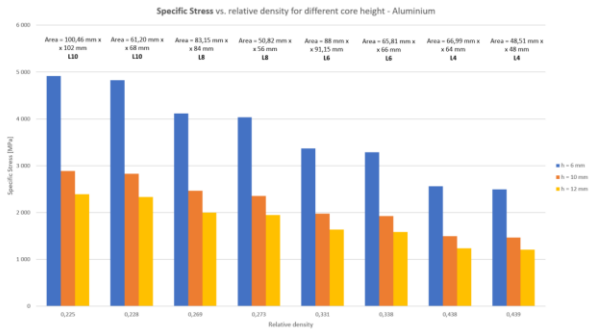

Figure 31 - Specific stress vs. relative density for aluminium regular structures – Numerical analysis.

4. Conclusions

The honeycomb structures are the most used core solution when it comes to sandwich panels. The high strength-to-weight ratio makes this type of structure very attractive for many applications, making it of wide use throughout many areas of industry. Emerging Additive Manufacturing techniques allows the use of new materials and facilitates the production of more complex geometries. One of the main assets (besides the strength-to-weight ratio) is the high energy absorption capacity, which can be further enhanced through the design of functionally graded structures. This design can be approached either by material's composition changes or by morphological changes. This work intended to design FGM structures by the introduction of geometrical gradients, being the cell walls' thickness-to-length ratio, the chosen project parameter.

The studies on this work comprised the analysis of uniform (regular structures) and graded wall thickness. In other works that have studied honeycomb structures [19, 20], the specimen size has been pointed as one of the factors that influences the behaviour of the structures when it comes to energy absorption and strength. It was possible to conclude that the overall size of the structure and the length-to-thickness ratio are the main factors to influence the out-of-plane mechanical behaviour of the honeycomb structures: larger structures with higher relative densities (the last one expressing the length-to-thickness ratio) enhance their stiffness and energy absorption capacity, as well as their strength. Also, graded structures have their stiffness, energy absorption and strength improved due to the mass distribution: structures that benefit from a larger mass concentration near the centre have their out-of-plane mechanical properties improved.

Relatively to the potential of Additive Manufacturing for the mentioned structures, the development of tailored sandwich panels cores, such as the functionally graded honeycombs, impose significant geometrical requirements of the manufacturing processes used to produced them. Considering so, the design freedom allowed by AM technologies surge as a natural solution for their production and continuous development. Additionally, future developments should take into consideration process constraints as early as possible in the design process, taking advantage of methodologies such as design for additive manufacturing.

In what concerns to the PLA specimens, there was a good correspondence between numerical and experimental results, validating Fused Filament Fabrication process as an alternative to produce design prototypes of graded cellular materials. Regarding the Selective Laser Melting technique, it isn't possible to make any definite statement due to the incongruent results on aluminium specimens.

Finally, a very good match of results was found between the Finite Element Analysis results and the experimental testing ones. The correlation between both results makes possible to state that the Finite Element Method is an excellent tool when it comes to the analysis of this type of structures.

References

[1] K. K. Chawla, Composite Materials: Science and Engineering, 4th ed., Springer, 2019.

[2] V. Birman and G. A. Kardomateas, "Review of current trends in research and applications of sandwich structures," *Composites Part B: Engineering,* vol. 142, pp. 221-240, 2018.

[3] H. Araújo, M. Leite, A. M. R. Ribeiro, A. M. Deus, L. Reis and M. F. Vaz, "Investigating the contribution of geometry on the failure of cellular core structures

obtained by additive manufacturing," *Frattura ed Integrità Strutturale,* vol. 13, pp. 478-486, 2019.

[4] A. Miranda, M. Leite, L. Reis, E. Copin, M. F. Vaz and A. M. Deus, "Evaluation of the influence of design in the mechanical properties of honeycomb cores used in composite panels," *Journal of Materials: Design and Applications,* vol. 235, pp. 1325-1340, 2021.

[5] J. Bru, M. Leite, A. R. Ribeiro, M. F. Vaz and A. M. Deus, "Bioinspired structures for core sandwich composites produced by fused deposition modelling," *SAGE Journals,* vol. 234, pp. 379-393, 2020.

[6] J. G. Monteiro, M. Sardinha, F. Alves, A. R. Ribeiro, L. Reis, A. M. Deus, M. Leite and M. F. Vaz, "Evaluation of the effect of core lattice topology on the properties of sandwich panels produced by additive manufacturing," *Journal of Materials: Design and Applications,* vol. 235, pp. 1312-1324, 2020.

[7] R. Kamalieva and R. Charkviani, "Creation of Ultra-light Spacecraft Constructions Made of Composite Materials," *Procedia Engineering,* vol. 185, pp. 190-197, 2017.

[8] I. Carranza, A. Crocombe and I. Mohagheghian et al., "Characterising and modelling the mechanical behaviour of polymeric foams under complex loading," *J Mater Sci,* vol. 54, pp. 11328-11344, 2019.

[9] L. Gibson and M. Ashby, Cellular Solids: Structure and Properties, 2nd ed., Cambridge University Press, 1997.

[10] T. Bitzer, Honeycomb Technology: Materials, Design, Manufacturing, Applications and Testing, 1st ed., Chapman & Hall, 1997.

[11] S. H. Goodman and H. Dodiuk, Handbook of Thermoset Plastics, 3rd ed., Elsevier, 2014.

[12] D. Bathe, C. A. Penick, L. A. Ferry and C. Lee, "Classification and Selection of Cellular Materials in Mechanical Design: Engineering and Biomimetic Approaches," *Designs,* vol. 3, 2019.

[13] I. Gibson, D. Rosen, B. Stucker and M. Khorasani, Additive Manufacturing Technologies, 3rd ed., Springer, 2021.

[14] M. Attaran, "The rise of 3-D printing: The advantages of additive manufacturing over traditional manufacturing," *Business Horizons,* vol. 60, pp. 677-688, 2017.

[15] I. Bahnini, M. Rivette, A. Rechia, A. Siadat and A. Elmesbahi, "Additive manufacturing technology: the status, applications and prospects," *The International Journal of Advanced Manufacturing Technology,* vol. 97, pp. 147-161, 2018.

[16] J. Gardan, "Additive manufacturing technologies: state of the art and trends," *International Journal of Production Research,* vol. 54, pp. 3118-3132, 2015.

[17] ASTM C365-94 standard, *Standard test method for flatwise compressive properties of sandwich cores.*

[18] B. G. M. Silva, "Cellular structures for use in composite panels with a mass distribution gradient produced by additive manufacturing," MSc dissertation, Instituto Superior Técnico - University of Lisbon, 2021.

[19] Y. Zhang, M. Lu, C. H. Wang, G. Sun and G. Li, "Out-of-plane crashworthiness of bio-inspired self-similar regular hierarchical honeycombs," *Composite Structures,* vol. 144, pp. 1-13, 2016.

[20] B. Yu, S. N. Khaderi, V. S. Deshpande and N. A. Fleck, "The effect of matrix shear strength on the out-of-plane compressive strength of CFRP cross-ply laminates," *International Journal of Solids and Structures,* vol. 139, pp. 79-95, 2018.